Effect of Cation Substitution on the Adsorption of Xenon on Zeolite NaY and on the Xenon-129 Chemical Shifts†

Shang-Bin Liu,* B. M. Fung,‡ Tran-Chin Yang, Eng-Chin Hong,§ and Chau-Ting Chang⊥

Institute of Atomic and Molecular Sciences, Academia Sinica, P. O. Box 23-166, Taipei, Taiwan 10764, Republic of China

Pei-Chin Shih, Fu-Hsing Tong, and Tun-Li Chen

Department of Chemistry, Tamkang University, Tamsui, Taiwan 25137, Republic of China

Received: January 24, 1994®

A comprehensive study of the effect of cation substitution on the adsorption of xenon on NaY zeolites and on ^{129}Xe chemical shifts has been made. The cations studied include H^+, alkali (Li^+, K^+, Rb^+, Cs^+), alkaline earth (Mg^{2+}, Ca^{2+}, Sr^{2+}, Ba^{2+}), and transition metal (Co^{2+}, Ni^{2+}, Cu^{2+}, Zn^{2+}), each with varied degree of exchange with Na^+. The results of the adsorption isotherms were analyzed by the use of a Langmuir-type equation. It was found that the adsorption strength for the Y-zeolites follows the trend Ba > Cs ≥ Rb > K ≥ Sr > Ca > Na ≥ Co ≥ Ni ≥ Li ≥ Zn > Cu ≃ H > Mg. The observed ^{129}Xe chemical shifts of the adsorbed xenon were interpreted by a newly developed virial expansion model; an equation relating the ^{129}Xe chemical shift and the amount of xenon atoms adsorbed per cage has been derived and used to fit the experimental data of all the systems studied, and the results are quite satisfactory. It is suggested that the adsorption strength and the ^{129}Xe chemical shift are dependent on the location of the cation in the supercage as well as on various interactions of the xenon atoms with each other and with the zeolite walls. The van der Waals interaction, which is determined by the polarizability of the interacting species, is the major interaction. The Coulombic interaction of the cations plays a secondary role.

Introduction

Because of the large polarizability of the xenon atom, the ^{129}Xe NMR chemical shift is very sensitive to its environment.[1] Therefore, ^{129}Xe NMR provides a sensitive probe for the investigation of the structure of zeolites. There have been numerous publications in this area since the first reports by Ito and Fraissard[2,3] and by Ripmeester,[4] and the subject has been reviewed in two recent articles.[5,6]

The three-dimensional framework of faujasite-type (X, Y) zeolites consists of TO_4 (T = Si, Al) tetrahedra linked by the shared oxygen atoms such that there are invariably two oxygen atoms for each T atom.[7-9] The anionic nature of the framework is generally caused by the substitution of Al for Si within the TO_4 tetrahedra and is locally neutralized by the presence of exchangeable cations within the interstices of the structure. For synthetic faujasite-type zeolites, there are 192 TO_4 tetrahedra in each unit cell; the value of the Si/Al ratio is in the range 1.0–1.5 for zeolite X and is >1.5–≃3.0 for zeolite Y. Cavities of three types are known to exist in these zeolites. The supercages (internal diameter ca. 1.3 nm) are confined by a tetrahedral arrangement of truncated octahedra through the connection of hexagonal prisms (small cavities formed by double six-membered oxygen rings or D6R) producing apertures 0.74 nm by means of 12-membered rings. The octahedra or sodalite units themselves enclosed cavities (internal diameter ca. 0.66 nm) in a further set called sodalite or β-cages with apertures of free diameter 0.23 nm. The distribution of cations in zeolites depends upon the presence of adsorbed water or hydroxyl groups, the Si/Al ratio, the thermal or hydrothermal pretreatment of the sample, and the nature of the exchangeable cation of the zeolites. Depending on the composition of the zeolite and the ionic radius, the cation M^+ or M^{2+} can be located in the supercages, the sodalite cages, or the hexagonal prisms. On the other hand, because of the large size of the xenon atom (kinetic diameter ~ 0.44 nm), it can only go into the supercages.

A systematic investigation of the effect of the cation on the chemical shift of ^{129}Xe adsorbed on zeolites has been carried out by Fraissard and co-workers.[2,3,5,10-15] They suggested an explanation of the ^{129}Xe chemical shift in terms of different contributions from xenon–xenon interactions and xenon–zeolite interactions. Cheung *et al.* has offered a more quantitative interpretation[16] by the use of a model in which the xenon atoms adsorbed on the wall of the supercage are in rapid exchange with those in the gaseous phase. However, neither group has treated the ^{129}Xe chemical shift data quantitatively to obtain parameters related to the nature of the cations.

We have carried out a detailed study of the effect of the substitution of Na^+ in zeolite NaY by other cations on the ^{129}Xe chemical shifts. The cations investigated include H^+, four group IA cations (Li^+, K^+, Rb^+, and Cs^+), four group IIA cations (Mg^{2+}, Ca^{2+}, Sr^{2+}, and Ba^{2+}), and four transition metal cations (Co^{2+}, Ni^{2+}, Cu^{2+}, and Zn^{2+}). We have analyzed the adsorption isotherms of xenon on the zeolite systems at 295 K and developed a virial expansion model to treat the ^{129}Xe chemical shifts quantitatively. In connection with these, the adsorption isotherms of xenon on the zeolite systems at 295 K have been analyzed. The parameters obtained from both the adsorption isotherm data and the ^{129}Xe chemical shift data are discussed in terms of the effect of the cations on various interactions of the xenon atoms with the zeolite supercage.

Experimental Section

Powdered, binderless NaY zeolite samples having Si/Al ratios of 2.49 and 2.57 were obtained from Strem Chemicals, Inc. Prior

† Presented, in part, at The International Symposium on Zeolites and Microporous Crystals, Nagoya, Japan, August 1993.

* Author to whom correspondence should be addressed. Telephone: (+)-886-2-3620212, ext. 219. Telefax: (+)886-2-3620200.

‡ Permanent address: Department of Chemistry, University of Oklahoma, Norman, OK 73019-0370.

§ Permanent address: Department of Chemical Engineering, Chenghsiu Junior College of Technology, Kaohsiung, Taiwan 83305, R.O.C.

⊥ Department of Chemistry, National Tsinghua University, Hsinchu, Taiwan 30043, R.O.C.

® Abstract published in *Advance ACS Abstracts,* March 15, 1994.

0022-3654/94/2098-4393$04.50/0

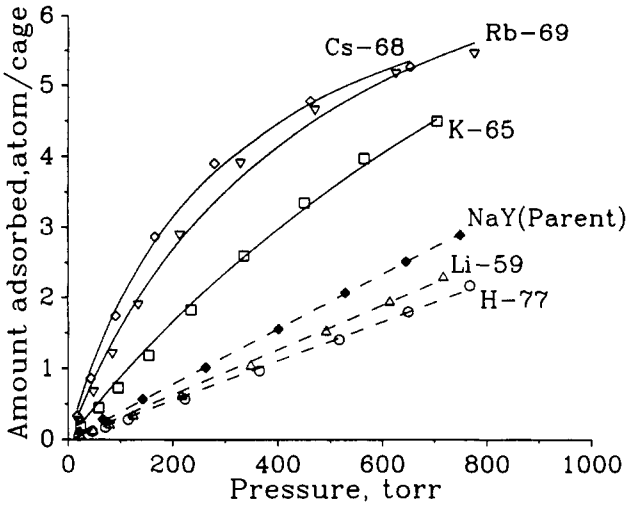

Figure 1. Room temperature (295 K) adsorption isotherms of xenon adsorbed on NaY zeolites with Na^+ partly replaced by various monovalent cations. The numbers indicate the percentage of Na^+ exchanged. The solid curves were calculated using eq 4; the dashed lines are empirical straight lines.

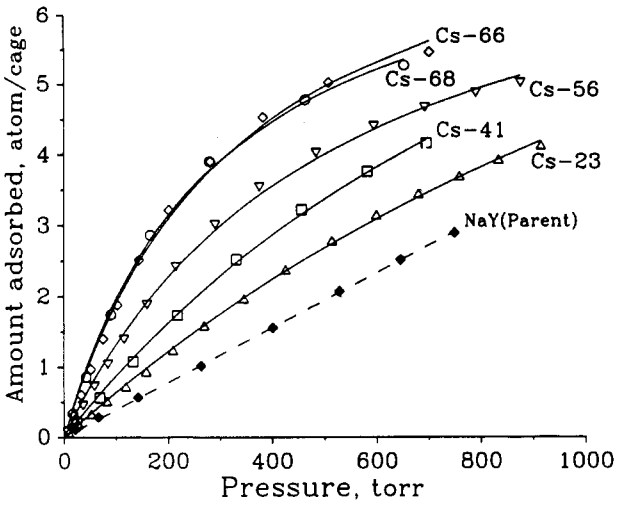

Figure 2. Room temperature adsorption isotherms of xenon adsorbed on NaY zeolites with Na^+ replaced by different amounts of Cs^+. The numbers indicate the percentage of Na^+ exchanged. The solid curves were calculated using eq 4; the dashed lines are empirical lines.

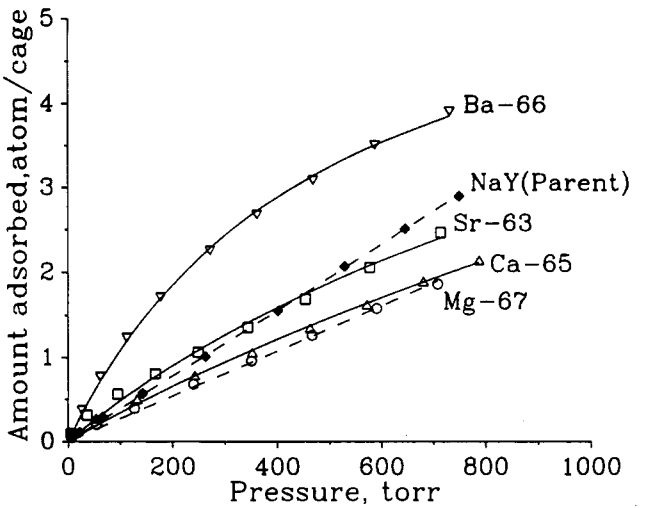

Figure 3. Room temperature adsorption isotherms of xenon adsorbed on NaY zeolites with Na^+ partly replaced by various group IIA bivalent cations. The numbers indicate the percentage of Na^+ exchanged. The solid curves were calculated using eq 4; the dashed lines are empirical straight lines.

to ion exchange, the parent NaY zeolites were sequentially washed with 1 mol dm^{-3} NaCl solution and deionized water and then dried at room temperature (295 K), to avoid possible deficiency in cations. Ion exchange was carried out by mixing the parent NaY zeolites with the appropriate chloride solution at room temperature. The ion-exchanged samples (hereafter denoted MNaY) were then washed with deionized water until the supernatant was free of Cl^- ions, air-dried, and stored over saturated NaCl solution in a desiccator.

To analyze the compositions of the ion-exchanged samples, a 0.1-g sample was digested with a mixture of hydrofluoric and nitric acids. Then, the product was heated and elemental analysis was carried out by the use of an inductive coupled plasma atomic emission spectrometer (Shimadzu GVM-1000) and a polarized Zeeman atomic adsorption spectrometer (Hitachi Z-6100).[17] The crystalline framework structure of the ion-exchanged zeolites was confirmed by X-ray diffraction (XRD) and by ^{27}Al magic-angle-spinning (MAS) NMR.

All the samples studied were dehydrated by gradual heating to 400 °C in vacuum (<10^{-5} Torr, 1 Torr = 133.32 Pa) and were then maintained at this temperature for at least 20 h before loading with xenon. Other details of the experimental procedure have been described elsewhere.[18-20] Under such dehydration condition, no traces of $M(OH)^+$ species can be found in MNaY zeolites (M = group IIA ions), as evidenced by separate FTIR (Bomem-DA8) measurements. Therefore, in this context, the effect of dissociation of H_2O by group IIA bivalent ions can be ignored.

The ^{129}Xe NMR experiments were performed at 83.012 MHz on a Bruker MSL-300 spectrometer as described previously.[18-20] All experiments were carried out at 295 K. The chemical shift of ^{129}Xe was referred to that of gaseous xenon at zero density according to an equation given by Jameson.[21,22] The resonance signal of ^{129}Xe adsorbed on all the zeolite samples shifts to higher frequency relative to the reference and is defined to be positive on the chemical shift scale.

The regressional and nonlinear least-squares fittings of the experimental data were done on a personal computer using a program developed by CSIRO Division of Mathematics and Statistics.

Results and Discussion

Xenon Adsorption Isotherms. The xenon adsorption isotherms on zeolite NaY and its homologues (MNaY), with Na^+ partly replaced by various monovalent cations, are shown in Figure 1. The isotherms for each ion, of course, depend upon the percentage of sodium ion exchanged. As an example, the effect for different percentages of Cs substitution is shown in Figure 2. The adsorption isotherms of NaY with group IIA bivalent cation substitutions are shown in Figure 3, and those for four transition metal cations are shown in Figure 4.

To interpret the adsorption isotherms quantitatively, we use the approach given by Cheung *et al.*[16] They suggested that the adsorption of xenon by NaY zeolites is dependent on the xenon density inside the supercage, ρ_g, according to the Langmuir relation:

$$\theta = \frac{b\rho_g}{1 + b\rho_g} \tag{1}$$

where θ is the fraction of sites occupied and b is the adsorption strength. Because ρ_g is not a directly measurable quantity, eq 1 is converted into another form by using the relations

$$\rho_g = \frac{N - N_s\theta}{V} = \rho - \frac{N_s\theta}{V} \tag{2}$$

and

$$\rho_g = rP \tag{3}$$

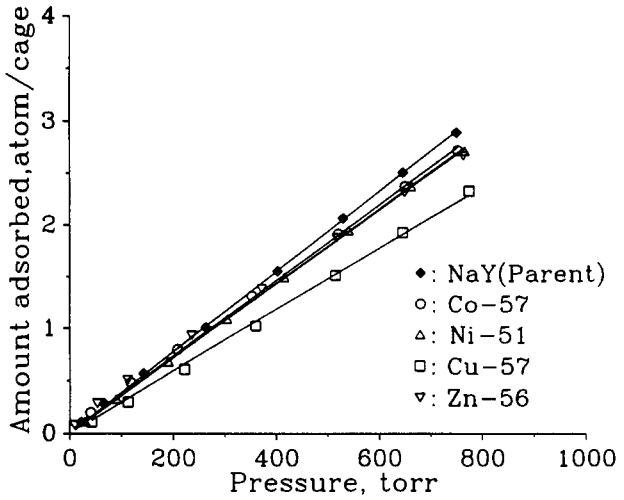

Figure 4. Room temperature adsorption isotherms of xenon adsorbed on NaY zeolites with Na^+ partly replaced by various transition metal cations. The numbers indicate the percentage of Na^+ exchanged. The lines are empirical straight lines.

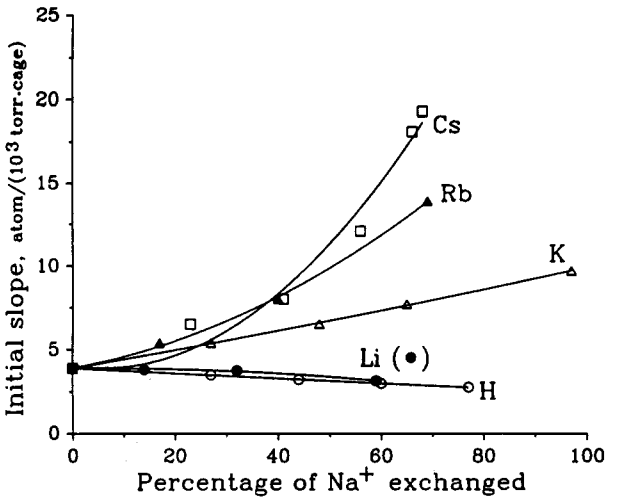

Figure 5. Initial slopes (m) of the xenon adsorption isotherms plotted against the percentage of Na^+ exchanged.

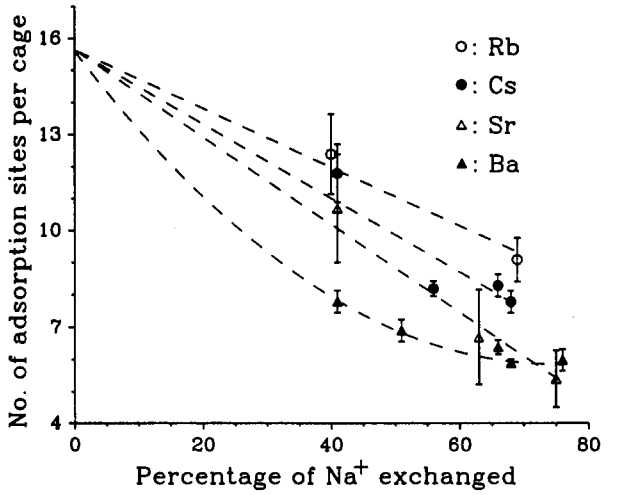

Figure 6. Total number of sites per cage calculated from the xenon adsorption isotherms plotted against the percentage of Na^+ exchanged. The lines are obtained from weighted least-squares fitting of the data to empirical second-order equations.

where N is the total number of xenon adsorbed in each zeolite supercage, V represents the free volume of the cage, $\rho = N/V$ is the total density of xenon, N_s is the total number of available sites per supercage, and P is the equilibrium pressure. The value of the proportionation constant r can be readily calculated according to the ideal gas law: $r = (kT)^{-1}$, where k is Boltzmann's constant and T is temperature. In this context, all experiments were carried out at $T = 295$ K and the value of $r = 3.2734 \times 10^{-5}$ atom nm^{-3} $Torr^{-1}$. Then, the total amount of xenon adsorbed, in a unit of atom $cage^{-1}$, is expressed by

$$N = r\left(V + \frac{bN_s}{1 + brP}\right)P \qquad (4)$$

At low surface coverage ($brP \ll 1$), the initial slope of the adsorption isotherm (i.e., near the Henry's law region) is

$$m = r(V + bN_s) \qquad (5)$$

For isotherms with appreciable curvatures, the parameters b and N_s can be obtained by least-squares fitting of the experimental data into eq 4 while keeping r and V as constants. The values of m were then calculated by eq 5. The effect of small variation in V for different MNaY has been proven to be negligible in the above treatment. At high surface coverage ($brP \gg 1$), $N = (N_s + rVP)$. Data obtained from the present experiments are given in Table 1 and plotted as solid curves in Figures 1–4.

To interpret the parameters obtained from fitting the adsorption isotherms, we would like to point out that there are a number of limitations in the model and experimental results. It is not certain that the Langmuir relation given by eq 1 is strictly applicable to a limited space such as the supercage of zeolite. Even if it is applicable, the adsorption isotherms presented as N versus P in eq 4 are only an approximation, because no distinction was made between weak and strong adsorptions, which will be discussed below. However, this approximation serves as a good starting point for the quantitative treatment of the adsorption of xenon on Y-type zeolites, and an analysis of the resulting parameters offers some insights to the nature of the adsorption with regard to the effect of the replacement of Na^+ by various ions.

The group IA metal ions show the largest variation in the values of the initial slopes (Figure 5). The values of N_s for NaY zeolites ion-exchanged with Rb, Cs, Sr, and Ba are plotted against the percentage of Na^+ exchanged in Figure 6, and the data are fitted to empirical second-order equations with a common intercept and appropriate weighting factors to obtain a value of $N_s = 15.6 \pm 0.5$ for parent NaY. Because isotherms for H, Li, Mg, Co, Ni, Cu, and Zn substitutions do not show any curvature at all, their values of N_s are assumed to be the same as that for NaY. The justification for this will be discussed below.

For MNaY zeolites, the volume V of the supercage would not change significantly with the replacement of Na^+ by other cations. For example, if all of the Na^+ ions are replaced by Cs^+, the largest cation we have studied, the value of V would decrease by only about 10%. On the other hand, the corresponding value of b increases notably from ~7 to as large as ~100 (Table 1, column 5). Moreover, for each MNaY sample, varying the value of V by ±10% only affects the values of both N_s and b by ca. 1%, which is within the error limit of the fitting.

Now let us discuss N_s, the number of adsorption sites per supercage, and its relation to the adsorption strength. For the parent NaY zeolite, the Na^+ ions are located in various sites in the supercages, the sodalite cages, and the hexagonal prisms.[7-9] A simple calculation shows that, for a Si/Al ratio of 2.5, there are 55 Na^+ ions per unit cell. From the results of X-ray diffraction and statistical calculations, it has been suggested that the preference of Na^+ at different sites in NaY is in the following order: site I > site II > site I'.[23-25] Considering this preference and the number of sites available for the cations,[7-9] we can deduce that there would be 16 of the Na^+ ions located in the hexagonal prisms (site I), 32 in the supercages (site II), and 7 in the sodalite cages (site I') in each unit cell. Since there are 8 supercages per unit cell, each supercage has 4 Na^+ ions. The other 42% of the Na^+ ions are located in the hexagonal prisms and/or sodalite cages, which will be designated as small cages as a whole.

TABLE 1: Data Obtained from the Analysis of Adsorption Isotherms and ^{129}Xe NMR Chemical Shifts for Xenon Adsorbed on Zeolite NaY with Na^+ Partly Replaced by Different Ions[a]

	ion exchange percentage	N_s, atom cage^{-1}	initial slope (m), atom cage^{-1} (10^3 Torr)$^{-1}$	b, nm^3 atom^{-1}	σ_0, ppm	C_1, ppm cage^{-1} atom	C_2, ppm cage^{-1} atom^{-2}
Na	Si/Al = 2.49	15.6(0.5)[b]	3.88(0.02)	7.05(0.03)	56.9	14.78	–
	Si/Al = 2.57	15.6(0.5)	3.94(0.02)	7.65(0.03)	58.6	15.55	–
H	27	c	3.50(0.02)	6.80(0.03)	59.5	14.78	–
	44	c	3.22(0.04)	6.25(0.06)	61.3	14.79	–
	60	c	2.99(0.04)	5.80(0.07)	61.6	15.28	–
	77	c	2.76(0.03)	5.36(0.05)	63.3	14.88	–
Li	14	c	3.81(0.01)	7.41(0.04)	58.5	14.41	–
	32	c	3.77(0.01)	7.34(0.05)	57.8	14.45	–
	59	c	3.15(0.03)	6.12(0.06)	56.1	15.52	–
K	27	[14.3(1.0)][d]	5.4(0.2)	11.4(2.1)	64.6	13.75	–
	48	[13.9(0.6)][d]	6.5(0.2)	14.2(1.6)	68.9	12.85	–
	65	[13.5(1.0)][d]	7.7(0.2)	18.4(2.2)	71.0	12.19	–
	97	12.9(0.6)	9.7(0.2)	28.0(4.5)	76.9	10.57	–
Rb	17	[14.6(1.0)][d]	5.4(0.2)	11.5(1.7)	66.8	14.07	–
	40	12.4(1.1)	8.0(0.2)	23.4(2.9)	76.9	12.61	–
	69	9.1(1.4)	13.9(0.2)	64.1(7.8)	87.4	11.25	–
Cs	23	[13.1(0.6)][d]	6.5(0.2)	15.6(0.9)	76.5	14.05	–
	41	11.8(0.8)	8.0(0.2)	24.3(2.4)	88.9	13.27	–
	56	8.2(0.2)	12.1(0.2)	58.6(3.2)	105.2	12.82	–
	66	8.3(0.3)	18.1(0.2)	89.4(6.7)	121.4	10.91	–
	68	7.8(0.3)	19.3(2.0)	103.2(9.0)	125.8	11.73	–
Mg	44	c	2.85(0.02)	5.53(0.03)	63.1	11.30	3.04
	56	c	2.82(0.03)	5.47(0.03)	62.6	12.34	3.05
	61	c	3.27(0.03)	6.35(0.06)	69.1	3.01	4.19
	67	c	2.69(0.03)	5.21(0.06)	71.8	–2.28	8.53
Ca	38	[12.1(1.0)][d]	3.4(0.1)	9.0(1.0)	58.1	13.40	0.63
	61	[11.8(1.0)][d]	3.5(0.1)	10.0(1.0)	70.8	–0.63	4.98
	65	8.8(1.0)	3.3(0.1)	12.1(3.3)	90.1	–25.77	15.23
	71	6.8(1.3)	4.4(0.2)	20.7(5.4)	114.2	–32.42	12.52
Sr	41	10.7(1.5)	3.7(0.1)	11.2(2.4)	67.7	4.36	3.89
	63	6.7(1.3)	5.8(0.5)	23.3(6.1)	98.3	–8.92	5.07
	75	5.4(0.8)	6.3(0.3)	39.1(8.7)	113.4	–7.87	3.72
Ba	41	7.8(0.3)	6.1(0.2)	28.0(1.7)	112.2	5.11	–
	51	6.9(0.3)	8.7(0.5)	43.8(3.2)	118.3	5.68	–
	66	6.4(0.2)	10.8(0.5)	61.5(3.3)	123.1	6.55	–
	68	5.9(0.1)	11.5(0.7)	75.2(3.3)	124.6	7.29	–
	76	6.0(0.3)	13.2(0.2)	88.9(8.4)	123.9	7.24	–
Co	6	c	3.88(0.04)	7.54(0.03)	674.8	–414.89	80.90
	11	c	3.83(0.02)	7.45(0.03)	1199.5	–784.65	152.10
	26	c	3.72(0.03)	7.23(0.05)	1055.9	–706.37	142.28
	43	c	3.69(0.03)	7.17(0.04)	968.0	–640.88	130.64
	57	c	3.67(0.01)	7.13(0.06)	1156.8	–724.05	142.71
Ni	6	c	3.79(0.02)	7.36(0.02)	115.4	–16.07	5.63
	11	c	3.81(0.03)	7.41(0.03)	136.6	–25.15	7.05
	27	c	3.68(0.02)	7.15(0.03)	145.6	–32.01	8.96
	34	c	3.49(0.03)	6.79(0.05)	137.5	–23.90	7.78
	42	c	3.64(0.03)	7.08(0.03)	169.4	–51.30	15.27
	51	c	3.58(0.02)	6.96(0.02)	380.1	–176.80	37.05
Cu	6	c	3.74(0.03)	7.28(0.03)	59.6	14.35	–
	13	c	3.66(0.03)	7.11(0.04)	56.6	15.04	–
	28	c	3.51(0.02)	6.82(0.04)	51.7	15.86	–
	35	c	3.35(0.03)	6.50(0.03)	51.1	16.39	–
	49	c	3.21(0.03)	6.23(0.02)	47.6	17.15	–
	57	c	2.97(0.03)	5.75(0.06)	45.9	18.60	–
Zn	6	c	3.75(0.02)	7.29(0.02)	62.7	12.02	0.45
	11	c	3.67(0.04)	7.13(0.03)	61.8	12.60	0.36
	29	c	3.48(0.01)	6.76(0.03)	73.1	4.48	2.16
	36	c	3.40(0.01)	6.60(0.02)	76.2	2.79	2.53
	41	c	3.46(0.02)	6.71(0.05)	87.5	–5.10	4.13
	56	c	3.60(0.04)	6.99(0.12)	108.7	–16.49	5.84

[a] The values of N_s, b, and m are obtained by nonlinear least-squares fitting of eqs 4 and 5. The standard errors in the parentheses following each data were obtained from the least-squares calculations. The values of σ_0, C_1, and C_2 are obtained by regressional fitting of the experimental results to eq 10 from a second-degree polynomial. [b] From the extrapolated data; see Figure 6. [c] Assumed to be 15.6 atom cage^{-1}. [d] Interpolated values.

On the basis of the molecular dynamic simulations of xenon adsorption in NaY (Si/Al = 3.0), Yashonath and his co-worker showed[26-28] that, for a system of one xenon atom per cage and an average temperature of ca. 373 K, xenon moves mostly along the surface of the inner walls of the supercages throughout the process of cage-to-cage migration. They also revealed that the most favorable distance between the center of the cage and xenon atom is ca. 0.45 nm at which a minimum xenon–xenon interaction potential is located. This further indicated that the site-to-site migration is the rate-determining step for the diffusion of xenon in NaY. If one assumes that the supercage is roughly spherical with a diameter of 1.3 nm and the xenon atom has a diameter of 0.44 nm, the number of xenon atoms that can fully cover the inner surface of the sphere is about 15.3. However, because each supercage is connected to four others through large pores having apertures of 0.74 nm,[7-9] it is difficult to calculate the exact number of xenon atoms that can fully cover the walls of the zeolite interior. Woods and Rowlinson reported[29] a maximum xenon sorption capacity of 8 per cage of NaY (Si/Al = 3.0) on the basis of their grand canonical ensemble Monte Carlo simulations. However, the results of the Monte Carlo simulation do not agree with experimental data very well for pressure higher than 0.1 atm.

TABLE 2: Parameters for Various Cations (M) and for NaY Zeolites with 40% of Na^+ Substituted by Different Cations

cation (M)[p]			40% MNaY zeolites[a]			
type	valency p	ionic diameter,[b] nm	V,[c] nm^3 $cage^{-1}$	N_s, atom $cage^{-1}$	b, nm^3 $atom^{-1}$	σ_0, ppm
H	+1	0.120	0.840	15.6	6.38	60.8
Li	+1	0.148	0.834	15.6	6.98	57.3
Na	+1	0.204	0.827	15.6	7.20	58.1
K	+1	0.276	0.800	14.1	13.13	67.3
Rb	+1	0.298	0.782	12.4	23.40	76.9
Cs	+1	0.340	0.753	11.9	24.00	88.2
Mg	+2	0.144	0.834	15.6	5.55	63.0
Ca	+2	0.200	0.827	12.1	9.09	59.2
Sr	+2	0.232	0.820	10.9	11.65	66.2
Ba	+2	0.272	0.800	7.9	26.42	111.6
Co	+2	0.130	0.840	15.6	7.19	983.5
Ni	+2	0.140	0.834	15.6	7.00	161.4
Cu	+2	0.144	0.840	15.6	6.40	49.9
Zn	+2	0.120	0.840	15.6	6.70	85.2

[a] Mostly interpolated values. [b] Reference 38; tetrahedral coordination. [c] Reference 39; interpolated values.

Similar results were found for xenon adsorbed in NaY (Si/Al = 2.4) based on a BET adsorption model.[30] The BET model, which assumes multilayer adsorption on a flat surface, is not a good description of the adsorption of xenon inside the limited volume of the NaY supercage.

An alternative way of estimating the monolayer capacity is through the relationship with the specific surface S (in unit of m^2 g^{-1}),[31]

$$N_s = \frac{M}{N_0 A_m} S \qquad (6)$$

where N_0 is Avogadro's number, A_m is the molecular cross-sectional area of the adsorbate, and M is the molecular weight of the adsorbate. For comparison, the specific area of NaX (Si/Al = 1.33)[7] is 1400 m^2 g^{-1}, and for xenon, $A_m = 25 \times 10^{-20}$ m^2 (ref 31), M = 131.3 g mol^{-1}, one obtains a value of N_s = 14.9 atom $cage^{-1}$ when taking the calculated value of 3.77×10^{20} cage/g of adsorbent (NaY) into consideration. Since there are 4 Na^+ in each supercage, it is impossible for 1 Na^+ to attract 4 xenon atoms due to the difference in their sizes. Thus, the adsorption of xenon on NaY is mainly determined by the available surface area on the supercage, rather than by the presence of Na^+ on their surface.

For bivalent cations, the preference of the zeolite sites has the following order: site I > site I' > site II.[23-25] It has been reported that different types of small bivalent ions replacing Na^+ prefer going into the small cages,[32-37] up to 60% substitution.[33] Systems with H^+ and Li^+ substitution have been less well studied. Whether they prefer going inside the small cages like the bivalent cations or replace Na^+ randomly in both kinds of cages would not affect the volume of the supercage significantly. In any case, for the ions which do not show any curvature in the adsorption isotherms up to 800 Torr (Figures 1 and 4), the assumption of N_s = 15.6 ± 0.5 is quite reasonable.

The situation is different for the larger exchangeable cations. The diameter of the sodalite cages in NaY is about 0.66 nm, and the aperture of the hexagonal prisms is 0.23 nm.[7-9] It is difficult for ions with diameters larger than about 0.22 nm (K^+, Rb^+, Cs^+, Sr^{2+}, and Ba^{2+}; Table 2[38]) to enter these units; therefore, the large ions would be located in the supercages. Since the adsorption of xenon on zeolites is probably due mainly to van der Waals attraction, the increased polarizability of the electron-rich ions located in the supercages would favor the adsorption of xenon atoms and an increase of the adsorption strength. Thus, unlike Na^+, the strong adsorption of xenon on zeolites containing the large ions Rb^+, Cs^+, Sr^{2+}, and Ba^{2+} may be site-specific, with a one-to-one correspondence to the number of cations replacing Na^+. The limiting values of N_s at 100% substitution as calculated from the adsorption isotherm data are ~6 for Rb^+, ~5 for Cs^+, ~2 for Sr^{2+}, and ~5 for Ba^{2+} (Figure 6). We must note that the experiments were not carried out to very high percentages of substitution, and the corrleations shown in Figure 6 are purely empirical. Considering that these limiting values of N_s may have fairly large uncertainties, these numbers are consistent with the suggestion of the site-specific character of strong adsorption. With less than complete substitution, the observed values of N_s and b would be weighted averages for the strong and weak adsorptions. The cases for K^+ and Ca^{2+} appear to be intermediate, even though Ca^{2+} is quite small and can go inside the small cages.

In fitting our data with the Langmuir model (eqs 1–5), no attempt has been made to distinguish between weak (nonspecific) and strong (site-specific) adsorption. Experimentally, it is difficult to separate these two types of contributions. Therefore, the values of N_s and b given in Table 1 are only reasonable estimates rather than exact numbers. Nevertheless, the present study of the adsorption isotherms based on this simple model bears important implications in the interpretation of the ^{129}Xe chemical shift data, which will be discussed in the next section.

The algebraic values of the adsorption strength b and the initial slope m (Table 1) show the same trend, as expected. Although the values of N_s, b, and m listed in Table 1 exhibit certain fluctuations due to experimental uncertainties and the simplified nature of the treatment, some general trends can be observed. For group IA and IIA elements, the values of b and m increase with the increase of the percentage of Na^+ substitution, except for H and Li. For these elements and the transition metal cations, an opposite trend is observed. Because of the variations in the values of b for different kinds of cations (Table 1), for the convenience of discussion, we choose to use the least-squares interpolation of the data to 40% Na^+ replacement to compare the adsorption strength (Table 2). For a 40% substitution of the Na^+ ions, it is assumed that the ions H, Li, Mg, Ca, Co, Ni, Cu, and Zn are located inside the small cages[23-25,32-37] although the situation would not be significantly different if they actually replace Na^+ randomly in the small and large cages in a ratio of 3:4.[7-9] On the other hand, the ions K, Rb, Cs, Sr, and Ba would be located only in the supercage and not in the small cages due to the ionic size (Table 2). In addition, the volume of the supercage (V) is considered to stay unchanged when 40% of Na^+ is replaced by H, Li, Mg, Ca, Co, Ni, Cu, and Zn ions. On the other hand, V would decrease slightly when Na^+ is replaced by the large cations K^+, Rb^+, Cs^+, Sr^{2+}, and Ba^{2+} (Table 2). For example, with a 100% substitution of Na^+ by Cs^+ (diameter 0.340 nm, Table 2), there are at most 7 Cs^+ atoms in each supercage, and the value of V is reduced by ca 10%. For 40% substitution, there is less reduction in V.

The overall trend for the adsorption strength b is

$$Ba > Cs \geq Rb > K \geq Sr > Ca > Na \geq Co \geq Ni \geq Li \geq Zn > Cu \simeq H > Mg$$

It was pointed out previously that the major force responsible for the adsorption of xenon on zeolites is the van der Waals attraction. Therefore, the adsorption strength is greater for the larger and more polarizable ions which are located in the supercages. The Coulombic interaction is not likely to be a major factor, as indicated by the smaller values of b for smaller ions compared with those for larger ions with the same charge. However, it may have a secondary effect: Ba^{2+} is isoelectronic with Cs^+ but has a higher charge and larger adsorption strength. For ions located inside the small cages, the adsorption strength b stays in the range 6.0 ± 1.0 nm^3 $atom^{-1}$, which can be regarded as almost unchanged within the overall error limit of the calculation.

To look at the values of b in another way, the trend for the group IA ions is

$$Cs \geq Rb \gg K > Na > Li$$

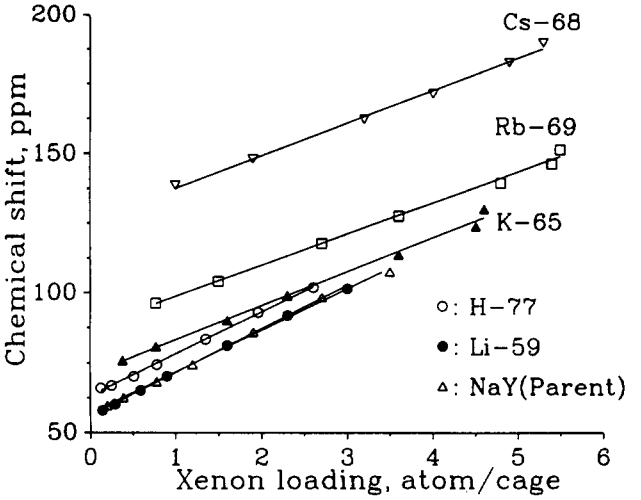

Figure 7. ^{129}Xe chemical shifts of xenon adsorbed on NaY zeolites with Na^+ partly replaced by various monovalent cations. The numbers indicate the percentage of Na^+ exchanged. The solid curves were calculated using eq 10; the dashed lines are empirical straight lines.

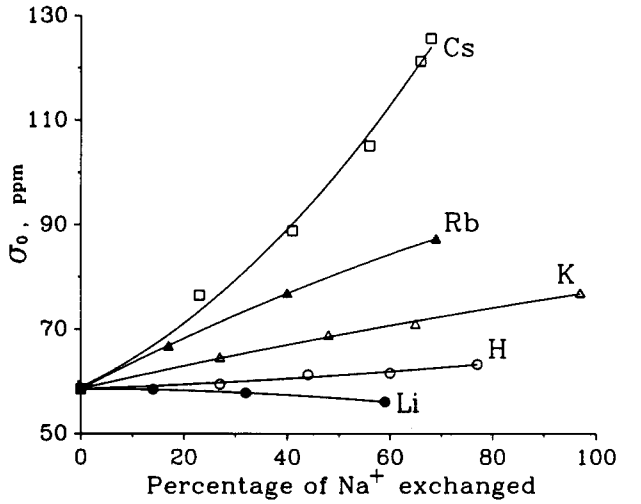

Figure 8. Dependence of ^{129}Xe chemical shift at zero xenon loading on the percentage of Na^+ exchanged.

and that for the group IIA ions is

$$Ba \gg Sr > Ca \gg Mg$$

They vary quite regularly with the sizes of the ions. This is easily understood due to the fact that the adsorption strength is a weighted average between the strong and weak adsorptions, and the large ions tend to locate in the supercage and are responsible for the strong adsorption.

^{129}Xe Chemical Shifts: A General Consideration. It has been observed for some time that, for NaY and its homologues with Na^+ being substituted by various monovalent cations, the ^{129}Xe chemical shifts vary linearly with xenon loading.[2,3,5] The slopes of the plots depend on the type and the extent of cation substitution (Figure 7). When the lines are extrapolated to zero xenon loading, the intercepts (σ_0) show a dependence on the percentage of Na^+ exchanged (Figure 8) remarkably similar to that for the slopes of the adsorption isotherms (Figure 5). For bivalent cations, the dependence of the ^{129}Xe chemical shift on xenon loading is not linear, except for Ba (Figure 9) and Cu (Figure 10).

The general features of the data presented in Figures 7, 9, and 10 agree well with those given by Ito and Fraissard.[2,3,5,10-15] They used the following expression to explain the dependence of ^{129}Xe chemical shifts on the replacement of Na^+ in NaY by various ions:

$$\delta = \delta_0 + \delta_s + \zeta_g \rho_g + \delta_e + \delta_m \qquad (7)$$

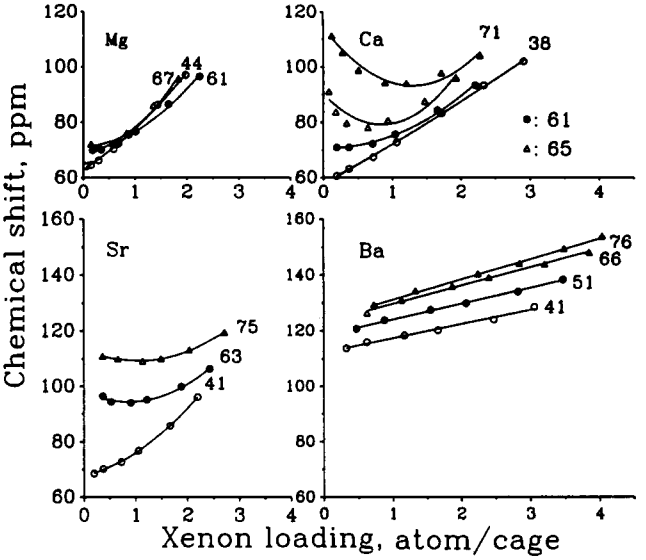

Figure 9. ^{129}Xe chemical shifts of xenon adsorbed on NaY zeolites with Na^+ partly replaced by various group IIA bivalent cations. The numbers indicate the percentage of Na^+ exchanged. The solid curves were calculated using eq 10.

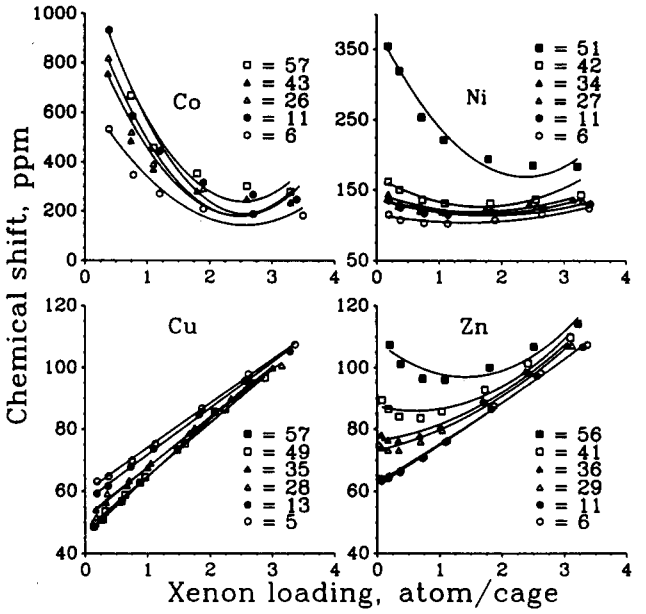

Figure 10. ^{129}Xe chemical shifts of xenon adsorbed on NaY zeolites with Na^+ partly replaced by various transition metal cations. The numbers indicate the percentage of Na^+ exchanged. The solid curves were calculated using eq 10.

where δ_0 is the reference, δ_s corresponds to the shift at zero xenon loading, $\zeta_g \rho_g$ is the xenon–xenon interaction term in the gaseous phase, δ_e is due to the "electric effect" caused by the cations, and δ_m is due to the "magnetic effect" of the paramagnetic ions. The equation can only give qualitative but not quantitative features about the complex dependence of the ^{129}Xe chemical shift on the type of cation and the percentage of Na^+ exchanged, as shown in Figures 7, 9, and 10.

More recently, Cheung *et al.* adapted a different approach[16] and suggested that the observed ^{129}Xe chemical shift is actually a weighted average between those of two species in rapid exchange, one adsorbed on the wall of supercage and another staying in the middle of the supercage like ordinary xenon gas:

$$\sigma = \delta - \delta_0 = \frac{N_s \theta}{N} \sigma_s + \left(1 - \frac{N_s \theta}{N}\right) \sigma_g \qquad (8)$$

where σ_s is the chemical shift of the adsorbed xenon atoms. By considering that the chemical shift of xenon in the gaseous phase, σ_g, changes linearly with its density (at low xenon loading),[21,22]

$$\sigma_g = \zeta_g \rho_g \tag{9}$$

they were able to derive an equation to explain why some of the chemical shift plots are linear (Figure 7), but some others are curved (Figures 9 and 10). However, no quantitative treatment of the data was given.

Besides the lack of quantitative data treatment, these models are discrepant with experimental results. Both groups of authors suggested that systems with weak adsorption strengths lead to a linear dependence whereas those with strong adsorption strengths yield parabolic plots. However, experimentally, four of the five systems with the largest adsorption strengths, K^+, Rb^+, Cs^+ and Ba^{2+}, give essentially linear plots (Figures 7 and 9). On the other hand, most of the systems showing upward concave curves (Ca^{2+} in Figure 9 and Co^{2+}, Ni^{2+} and Zn^{2+} in Figure 10) have very small adsorption strengths (Table 1). Moreover, upon a detailed examination, we found that the term involving σ_g in eq 8 contributes only ≤1% of the observed chemical shift (σ), while the dominant contribution of the ^{129}Xe chemical shift in the system is due to σ_s (the adsorbed xenon), which is dependent on the type of cation exchanged. Thus, a detailed quantitative description of the ^{129}Xe chemical shift cannot be easily obtained by eq 8. Obviously, a different approach must be sought so that the data can be interpreted and are consistent with results of the adsorption isotherm data.

^{129}Xe Chemical Shifts: The Virial Expansion Model. For a quantitative analysis of the dependence of the chemical shift (σ) on the amount of xenon adsorbed (N), we note that all the data can be nicely fitted with a second-order polynomial:

$$\sigma = \sigma_0 + C_1 N + C_2 N^2 \ldots \tag{10}$$

The results for σ_0, C_1, and C_2 are listed in Table 1 for each MNaY system; they are also shown in Figures 7, 9, and 10 as solid curves. Because the plots for the monovalent ions, Ba, and Cu are essentially linear, their C_2 values were taken as zero.

To understand the physical significance of the parameters σ_0, C_1, and C_2, we will use a model which treats the adsorbed xenon as a two-dimensional gas. If the major force responsible for the adsorption of xenon in zeolite is van der Waals interaction, the adsorbed xenon atoms can change their locations by moving around the surface of the supercage or by exchange with other xenon atoms in the gaseous phase. Then, there exist at least two types of adsorbed xenon: one in direct contact with the cage wall of the zeolite and the other not in such direct contact as shown in Figure 11. If the number of gaseous xenon atoms and the two types of adsorbed xenon atoms are denoted by N_g, N_d, and N_i, respectively, the total number of adsorbed xenon atoms in each zeolite supercage (N) is

$$N = N_d + N_i + N_g \tag{11}$$

and the observed chemical shift can be written as

$$\begin{aligned} \sigma &= f_d\sigma_d + f_i\sigma_i + f_g\sigma_g \\ &\simeq (1 - f_i)\sigma_d + f_i\sigma_i \end{aligned} \tag{12}$$

where f_d, f_i, and f_g refer to the fraction of the directly adsorbed, indirectly adsorbed, and gaseous xenon atoms, respectively. For simplicity, the term $f_g\sigma_g$ will be discarded in the future discussion; its contribution to the observed chemical shift (≤1%) is negligibly small within the numerical uncertainty of the treatment. The fraction of indirectly adsorbed xenon atoms, f_i, is expanded as a Taylor series of the surface coverage:

$$f_i = \beta_1\left(\frac{N}{N_s}\right) + \beta_2\left(\frac{N}{N_s}\right)^2 + \ldots \tag{13}$$

where the β values are the coefficients of the expansion. Also, we would express the ^{129}Xe chemical shifts for the two types of

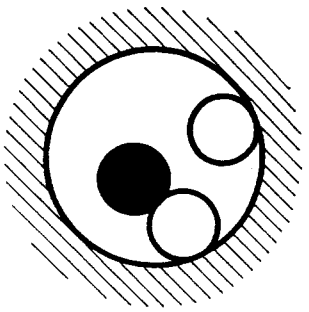

Figure 11. Schematic diagrams showing two types of adsorbed xenon atoms, namely, the directly adsorbed (open circle) and the indirectly adsorbed (full circle) xenon.

adsorbed atoms as a virial expansion, similar to that used by Jameson *et al.* for gaseous xenon,[21,22] as follows:

$$\sigma_d = \sigma_0 + \xi_1 N + \xi_2 N^2 + \ldots \tag{14}$$

and

$$\sigma_i = \xi_1 N + \xi_2 N^2 + \ldots \tag{15}$$

where σ_0, as before, denotes the effect of the zeolite surface on the chemical shift of the directly adsorbed xenon atoms in absence of xenon–xenon interactions (i.e., when $N \rightarrow 0$), and ξ_1 and ξ_2 are constants. When eqs 13–15 are substituted into eq 12, we obtain a second-order polynomial as expressed in eq 10, where

$$\begin{aligned} C_1 &= \xi_1 - \beta_1(\sigma_0/N_s) \\ C_2 &= \xi_2 - \beta_2(\sigma_0/N_s^2) \end{aligned} \tag{16}$$

Since the existence of more than two adsorbed layers of xenon is unlikely due to the limited size of the MNaY supercages, we shall not consider the higher order terms which involve mutual interactions of more than three xenon atoms.

In general, when the value of C_1 is positive, the plot of the ^{129}Xe chemical shift vs N is essentially linear (cf. Figure 7); the values of C_1 for these systems are roughly in the same order of magnitude as that obtained for the parent NaY. When the algebraic value of C_1 decreases or even becomes negative, the plot shows pronounced curvature (cf. Figures 9 and 10). The behaviors of C_1's allow us to predict the appearances of the plots which change with the size, charge valency, and percentage substitution of the cations. On the contrary, the algebraic value of C_2 is always positive. For those systems with non-zero C_2, the curvature in the plot is more pronounced when the algebraic value of C_2 increases.

To compare the values of σ_0 for different elements, we note that variations with the percentage of substitution of monovalent ions (Figure 8) are similar to those of another experimental quantity, the initial slope of the adsorption isotherms, m (Figure 5). It was noted earlier that the variations in the adsorption strength, b, also parallel those of m (Table 1). These comparisons lead to the logical conclusion that σ_0, the chemical shift of the directly adsorbed xenon in the absence of xenon–xenon interaction, is related to the adsorption strength.

For the data interpolated to 40% ion replacement, the values of σ_0 do not exhibit regular trends within each group (Table 2). To explain the variation in σ_0, we note that it would be related not only to the adsorption strength but also to small changes in the electron distribution of the xenon atom. In other words, although the Coulombic force of the ions plays a secondary role compared to the van der Waals attraction in determining the adsorption strength, it could influence the electron distribution of the directly adsorbed xenon atoms to change their chemical shift. For ions that are located inside the small cages, σ_0 exhibits the trend

$$Co \gg Ni \gg Zn > Mg > Ca \simeq H \simeq Na \simeq Li > Cu$$

The large effects of Co^{2+} and Ni^{2+} are undoubtedly due to their paramagnetic character; the unpaired electrons probably delocalize slightly in the zeolite framework and affect the adsorbed xenon atoms. The Zn^{2+}, Mg^{2+}, and Ca^{2+} ions are not paramagnetic; their effect on σ_0 is probably due to a combination of the +2 charge and the presence of the 3p and 3d electrons. The abnormal behavior of Cu is rather puzzling. To find out the reason for this behavior, separate experiments were performed on various of CuNaY samples to investigate the effect of Cu ions in the dehydrated, oxidized, reduced, and re-oxidized states using EPR (Bruker ER-300, X-band) in conjunction with ^{129}Xe NMR. The EPR spectra showed that the CuNaY samples do undergo partial autoreduction, as expected.[34] However, the ^{129}Xe NMR chemical shifts were independent of the valency of the Cu ion, having values similar to those plotted on Figure 10, upon dehydration, oxidation, reduction, and re-oxidation. These observations led us to conclude that, regardless of their valency, the Cu ions prefer to locate in the smaller cages rather than in the supercages of CuNaY zeolites. This would explain the smallest effect of Cu ion (among the systems studied) on the chemical shifts of the xenon atoms, which are located in the supercages.

For the ions located inside the supercages, σ_0 follows the trend

$$Ba > Cs > Rb > K \geq Sr$$

Again, it is interesting to note that this trend is almost the same as that for b (Table 2). Apparently, the dependence of σ_0 on the adsorption strength is more obvious for these ions, which can exert a more direct influence on the adsorbed xenon atoms.

Now let us consider the significance of the xenon–xenon interaction parameters C_1 and C_2, which are defined in eqs 10 and 16. Because we treat the adsorbed xenon as a two-dimensional gas, C_1 and C_2 are expected to be related to the adsorption coefficient b. However, because the directly and indirectly adsorbed xenon atoms interact with the surface of the supercage differently and there is no direct experimental method to distinguish between them, the value of b obtained from each adsorption isotherm fitting (Table 1) must be considered as a weighted average of the two types of adsorbed xenon atoms. These complications make it impossible to analyze the coefficients C_1 and C_2 in an analytical way. In the Appendix, we present an empirical treatment of the problem.

Conclusions

We have carried out a detailed investigation of the effect of ion exchange in NaY zeolites on the adsorption strength toward xenon atoms and on the change in the ^{129}Xe chemical shifts. Including Na^+ itself, a total of 14 different kinds of ions, each with 3–6 different percentages of exchange, have been investigated. The results of the adsorption isotherms were analyzed by the use of a Langmuir-type equation. We found that the dependence of the ^{129}Xe chemical shift on the amount of xenon adsorbed can be fitted with a second-order polynomial in all cases. This is interpreted by treating the adsorbed xenon as a two-dimensional gas with a virial expansion model similar to the case of xenon in the normal gaseous state.

When we consider the available data with 40% substitution of Na^+, we conclude that the small cations (H^+, Li^+, Mg^{2+}, Ca^{2+}, Co^{2+}, Ni^{2+}, Cu^{2+}, and Zn^{2+}) are located inside the small cages of the NaY zeolite systems, and the larger ions (K^+, Rb^+, Cs^+, Sr^{2+}, and Ba^{2+}) are located in the supercage. Our model takes into account the effects of the adsorption strength, the chemical shift of the adsorbed xenon, and the interaction between the gaseous xenon atoms and the cage wall. According to this model, the major force for the adsorption and various kinds of interaction of xenon in zeolites is the van der Waals force, but the Coulombic force of the cations also plays a secondary role. For Co^{2+} and Ni^{2+}, the paramagntic effect dominates the contributions to the ^{129}Xe chemical shifts.

In conclusion, the ^{129}Xe chemical shift of xenon adsorbed on zeolites is dependent on various interactions of xenon with its environments as well as the overall adsorption strength of the zeolite. Our new virial expansion model presented here combines the basic features of Ito and Fraissard's model, Cheung's model, and that of Jameson's treatment for gaseous system.[22] Although there are approximations and limitations in this model, it allows us to explain the results of a large number of systems quite well and sheds new light on the nature of ^{129}Xe chemical shifts of adsorbed xenon in zeolitic systems.

Acknowledgment. We dedicate this paper to the late Professor C. T. Chang, who died unexpectedly during the preparation of the manuscript. The support of this work by the National Science Council of the Republic of China, Grant Nos. NSC82-0208-M001-047 and NSC83-0208-M001-092, is gratefully acknowledged. We thank Professor Hellmut G. Karge and Dr. T. T. P. Cheung for stimulating discussions and Mr. H. C. Lin and Mr. T. H. Chen for their technical assistances. B.M.F. acknowledges the support of the National Science Council of the Republic of China for a Visiting Research Professorship at the Institute of Atomic and Molecular Sciences, Academia Sinica.

Appendix

In making quantitative analyses of C_1 and C_2, we introduce two empirical relations for the coefficients β in eq 13, such that

$$\beta_1 = \frac{\gamma_1}{b^\mu}, \qquad \beta_2 = \frac{\gamma_2}{b^\nu} \tag{A1}$$

where γ_1, γ_2, μ, and ν are constants. By substituting eq A1 into eq 16, we have

$$C_1 = \xi_1 - \frac{\gamma_1 \sigma_0}{b^\mu N_s} \quad \text{(in unit of ppm cage atom}^{-1}\text{)} \tag{A2}$$

and

$$C_2 = \xi_2 - \frac{\gamma_2 \sigma_0}{b^\nu N_s^2} \text{ (in unit of ppm cage atom}^{-2}\text{)} \tag{A3}$$

The values of C_1 and C_2 can then be fitted to eqs A2 and A3 independently by the use of nonlinear least-squares calculations with three variable parameters each: ξ_1, γ_1, and μ for the former and ξ_2, γ_2, and ν for the latter. The remaining parameters in eqs A2 and A3, namely, σ_0, b, and N_s, were held constant for each respective MNaY sample (Table 1).

When all 14 sets of C_1 data were fitted to eq A2, we obtained the values of $\xi_1 = 58.4 \pm 2.0$ ppm cage atom^{-1}, $\gamma_1 = 36.2 \pm 2.4$, and $\mu = 0.6$ with standard deviation of residuals (SDR) = 11.53. A smaller value of SDR generally means a better fitting quality. Similarly, when all 6 sets of non-zero C_2 values were pooled to fit eq A3, we obtained the values of $\xi_2 = -9.3 \pm 1.0$ ppm cage atom^{-2}, $\gamma_2 = -438.7 \pm 82.9$, and $\nu = 1.3 \pm 0.1$ with SDR = 3.71. The correlation between the calculated values C'_1 and C'_2 and the experimental values C_1 and C_2 is depicted in Figures 12 and 13, respectively. With the view that the types of systems studied were very comprehensive, the range of the chemical shifts covered was very wide, and a single equation with only three variable parameters was used for all systems, the quality of the fitting can be regarded as rather satisfactory.

It is interesting to compare the value of ξ_1 obtained for xenon adsorbed in MNaY zeolites to the binary interaction parameter for gaseous xenon. Taking the value of $\xi_1 = 58.4$ ppm cage atom^{-1} and $V = 0.827$ nm^3 cage^{-1} (ref 39), we have $\xi_1 V = 48$ ppm nm^3 atom^{-1}, which is of the same order of magnitude as ζ_g obtained by Jameson *et al.* (20.7 ppm nm^3 atom^{-1}).[21,22] Alternatively, one

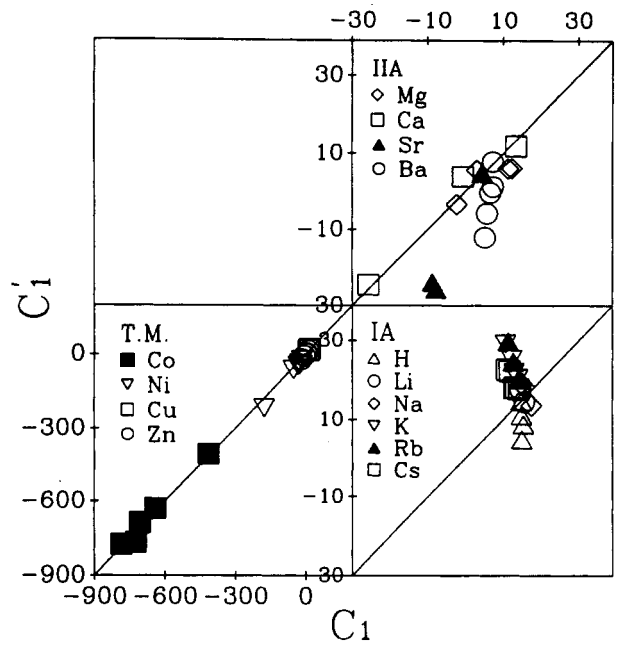

Figure 12. Plot of C_1 vs C'_1 for all of the MNaY samples examined. The solid line across the diagonal axis represents a perfect match between the fitted and calculated values. Note that the scales of the plots on the right-hand side have been expanded to avoid overcrowding of the symbols.

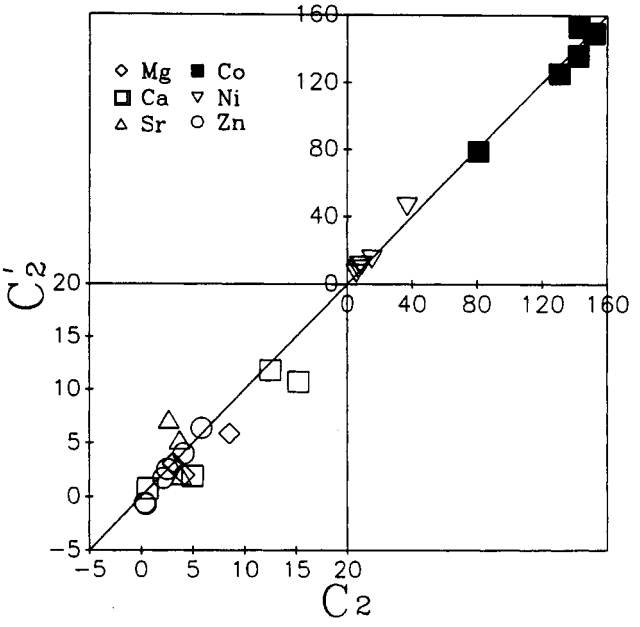

Figure 13. Plot of C_2 vs C'_2 for all of the MNaY samples with non-zero C_2 values (see Table 1). The solid line across the diagonal axis represents a perfect match between the fitted and calculated values.

can also use the value of ξ_1 to calculate the "apparent density" of the adsorbed xenon in the supercage using the relation $\sigma_0 \simeq \xi_1 V \rho_{Xe}$. For example, the average value of σ_0 is 58.8 ppm for the parent NaY (Table 1), yielding ρ_{Xe} = 1.22 atom nm^{-3} or 45 amagat (1 amagat = density of gas at 0 °C and 1 atm). This compares well with the value of 55 amagat obtained by Ito and Fraissard from a crude calculation based on mean-free-path theory.[3] The significance of ξ_2 is more difficult to assess: in contrast to the virial coefficients for gaseous xenon,[21,22] the sign of ξ_2 is opposite that of ξ_1. However, we note that in the case of xenon adsorbed in zeolites the space of the supercage is rather limited, hence the three-particle interaction likely involves two strongly adsorbed xenon atoms. The nature of this interaction compared to the three-particle interaction in xenon gas can probably be better understood by a detailed theoretical study.

Finally, we would like to point out that the interactions presented in Figure 11 and eq 12 (and hence eqs A2 and A3) are simplifications: the walls of the zeolite supercage are not uniform and are likely to be different for various group of MNaY. Therefore, the parameters ξ_1, γ_1, ξ_2, γ_2, μ, and ν need not have a single value. Moreover, there are considerable uncertainties in the experimental data due to sample variations and inaccuracies in the measurements. For example, the accuracy of the values of the ^{129}Xe chemical shifts is limited by the line widths, which increase from about 160 Hz for parent NaY to about 10 kHz with high percentages of Co^{2+} and Ni^{2+} substitutions. Nonetheless, even with the limitations discussed above, we believe that the virial expansion model has virtues over existing models. It gives reasonable and meaningful quantitative description of the MNaY systems studied.

References and Notes

(1) Reisse, J. *Nouv. J. Chim.* **1986**, *10*, 665.

(2) Ito, T.; Fraissard, J. In *Proceedings of the 7th International Zeolite Conference*; Rees, L. V. C., Ed.; Heyden: London, 1980; pp 510–515.

(3) Ito, T.; Fraissard, J. *J. Chem. Phys.* **1982**, *76*, 5225.

(4) Ripmeester, J. A. *J. Am. Chem. Soc.* **1982**, *104*, 289.

(5) Fraissard, J.; Ito, T. *Zeolites* **1988**, *8*, 350.

(6) Barrie, P. J.; Klinowski, J. *Prog. NMR Spectro.* **1992**, *24*, 91.

(7) Breck, D. W. *Zeolite Molecular Sieves: Structure, Chemistry, and Use*; Wiley: New York, 1974.

(8) Breck, D. W. *J. Chem. Educ.* **1964**, *41*, 678.

(9) Smith, J. V. *Adv. Chem. Ser.* **1971**, *101*, 171.

(10) Spriguel-Huet, M. A.; Ito, T.; Fraissard, J. In *Structure and Reactivity of Modified Zeolites*; Jacobs, P., Ed.; Elsevier: Amsterdam, 1984; pp 13–20.

(11) Fraissard, J.; Ito, T.; Spriguel-Huet, M.; Demarquay, J. In *Proceedings of the 7th International Zeolite Conference*; Murakami, Y., Iijima, A., Ward, J. W., Eds.; Kodansha-Elsevier: Tokyo, 1986; pp 393–400.

(12) Ito, T.; Fraissard, J. *J. Chim. Phys.* **1986**, *83*, 441.

(13) Ito, T.; Fraissard, J. *J. Chem. Soc., Faraday Trans. 1* **1987**, *83*, 451.

(14) Gedeon, A.; Bonardet, J. L.; Ito, T.; Fraissard, J. *J. Phys. Chem.* **1989**, *93*, 2563.

(15) Chen, Q. J.; Fraissard, J. *J. Phys. Chem.* **1992**, *96*, 1809.

(16) Cheung, T. T. P.; Fu, C. M.; Wharry, S. *J. Phys. Chem.* **1988**, *92*, 5170.

(17) Chao, K. J.; Chen, S. H.; Yang, M. H. *Fres. Z. Anal. Chem.* **1988**, *311*, 418.

(18) Liu, S. B.; Wu, J. F.; Ma, L. J.; Lin, M. W.; Chen, T. L. *Coll. Czech. Chem. Commun.* **1992**, *57*, 718.

(19) Wu, J. F.; Chen, T. L.; Ma, L. J.; Lin, M. W.; Liu, S. B. *Zeolites* **1992**, *12*, 86.

(20) Liu, S. B.; Ma, L. J.; Lin, M. W.; Wu, J. F.; Chen, T. L. *J. Phys. Chem.* **1992**, *96*, 8120.

(21) Jameson, A. K.; Jameson, C. J.; Gutowsky, H. S. *J. Chem. Phys.* **1970**, *53*, 2310.

(22) Jameson, C. J. *J. Chem. Phys.* **1975**, *63*, 5296.

(23) Dendooven, E.; Mortier, W. J.; Uytterhoeven, J. B. *J. Phys. Chem.* **1984**, *88*, 1916.

(24) Van Dun, J. J.; Mortier, W. J. *J. Phys. Chem.* **1988**, *92*, 6740.

(25) Van Dun, J. J.; Dhaeze, K.; Mortier, W. J. *J. Phys. Chem.* **1988**, *92*, 6747.

(26) Yashonath, S.; Santikary, P. *Phys. Rev. B* **1992**, *45*, 10095.

(27) Yashonath, S. *J. Phys. Chem.* **1991**, *95*, 5877.

(28) Yashonath, S. *Chem. Phys. Lett.* **1991**, *177*, 54.

(29) Woods, G. B.; Rowlinson, J. S. *J. Chem. Soc., Faraday Trans. 2* **1989**, *85*, 765.

(30) Shy, D. S. Ph.D. Thesis, Department of Chemistry, National Tsing-Hua University, Taiwan, R.O.C., 1992.

(31) Gregg, S. J. and Sing, K. S. W. *Adsorption, Surface Area and Porosity*; Academic Press: New York, 1967; Chapter 2.

(32) Gallezot, P.; Imelik, B. *J. Phys. Chem.* **1973**, *77*, 652.

(33) Otsuka, K.; Manda, J.; Morikawa, A. *J. Chem. Soc., Faraday Trans. 1* **1981**, *77*, 2429.

(34) Jacobs, P. A.; De Wilde, W.; Schoonheydt, R. A.; Uytterhoeven, J. B. *J. Chem. Soc., Faraday Trans. 1* **1976**, *72*, 1221.

(35) Suzuki, M.; Tsutsumi, K.; Takahashi, H.; Saito, Y. *Zeolites* **1988**, *8*, 381.

(36) Suzuki, M.; Tsutsumi, K.; Takahashi, H.; Saito, Y. *Zeolites* **1989**, *9*, 98.

(37) Godber, J.; Baker, M. D.; Ozin, G. A. *J. Phys. Chem.* **1989**, *93*, 1409.

(38) Shamron, R. D.; Prewitt, C. T. *Acta Crystallogr.* **1969**, *B25*, 925.

(39) Ramamurthy, V.; Eaton, D. F.; Caspar, J. V. *Acc. Chem. Res.* **1992**, *25*, 299.